PHASE-FIELD MODELING OF DENDRITIC GROWTH WITH CONVECTION

Christoph Beckermann*, Xinglin Tong* & Alain Karma**
*Department of Mechanical Engineering, University of Iowa, Iowa City, IA 52242, USA
**Department of Physics, Northeastern University, Boston, MA 02115, USA.

Summary A phase-field method is presented for modeling of solidification microstructure development with convection in the melt. The phase-field method relies on the introduction of a thin but numerically resolvable diffuse interface region and solves a transport equation for the phase-field variable that satisfies the Gibbs-Thomson interface condition implicitely. The method for convection includes a distributed momentum sink term to model the no-slip condition for the diffuse interface. The method is validated for several limiting cases involving flow through complex structures. Results are presented for equiaxed dendritic growth of a pure substance. The effects of convection on the dendrite tip operating state and the sidebranching are investigated in some detail.

INTRODUCTION AND DESCRIPTION OF METHOD

Convection usually accompanies solidification. Convection not only alters the microstructure of the solid that is forming, but solidification can also cause new and unexpected flow patterns. An example are the coupled morphological and convective instabilities investigated by Coriell et al. and Davis et al. Solidification pattern formation in the limit of purely diffusive transport of heat and/or solute has been studied extensively. The nonlinear interactions between solidification and convective transport, on the other hand, have received comparably little research attention.

The phase-field method has recently emerged as a viable tool to numerically simulate solidification microstructure development. In this method, a phase indicator function is introduced that varies smoothly from a constant value in the liquid phase to another constant value in the solid phase across a finite, but numerically resolvable diffuse interface region. A transport equation for the phase-field variable can be derived from basic thermodynamic considerations, or directly from the Gibbs-Thomson condition at a solid/liquid interface, including curvature and kinetic effects. This transport equation is solved in conjunction with conservation equations for heat, mass, and momentum on a fixed grid. The same equations apply in all regions of the domain and the interface is represented as volumetric sources in the conservation equations (e.g., as a distributed latent heat source). The main advantages of the phase-field method are that the explicit calculation of interface velocities, normals, and curvatures is completely avoided, there is no need to track the interface, and there is no need for iterations to satisfy interfacial boundary conditions.

We have recently extended the phase-field method to include convection in the melt[1,2]. Based on volume averaging, we have derived conservation equations that contain the phase-field variable and are equally valid in the solid, the liquid, and the diffuse interface region. Here a key issue is how the usual no-slip condition at a sharp solid/liquid interface is handled in the presence of the diffuse interface introduced by the phase-field method. For this purpose we have derived a volumetric momentum sink term in the Navier-Stokes equations that is proportional to the interfacial area and the liquid velocity. Across the diffuse interface region, the velocity pre-factor in the sink term increases from zero in the liquid to a large value in the solid, such that the velocity approaches zero in the fully solid region. The magnitude and variation of the velocity pre-factor is chosen through an asymptotic analysis, such that the velocity profile for plane flow past the diffuse interface matches the one for

flow past a sharp interface regardless of the thickness of the diffuse interface region. The effectiveness and accuracy of this approach is demonstrated for several test cases involving flows through regular arrays of cylinders for which analytical solutions are available.

We solved the phase-field and conservation equations using a multigrid method for the flow. Typically, six grid points are present in the diffuse interface, and the total number of grid points can reach several million in two dimensions. Convergence of the solution and grid anisotropy effects were investigated through detailed numerical tests. In particular, tests were conducted to ensure that the numerical results are independent of the thickness of the diffuse interface, and that in the limit of purely diffusive heat transport we recover available analytical solutions for dendrite tip growth.

RESULTS AND DISCUSSION

We present results for two-dimensional growth of a single equiaxed dendrite of a pure substance into an initially uniformly supercooled melt. A small spherical seed is initially present in the centre of the domain. The principal growth directions of the dendrite are aligned with the x-y coordinate axes. The liquid melt enters from the top boundary with a uniform inlet velocity and leaves at the bottom boundary. Symmetry conditions are applied at the sidewalls. The inlet and initial temperature are both set to some dimensionless supercooling.

For a fixed dimensionless supercooling of 0.55, Figure 1 shows the computed evolution of the dendrites for three different anisotropy strengths (ε=0.01, 0.03, and 0.05) without flow (top panels) and with flow (bottom panels). The flow Peclet number based on the inlet velocity and the capillary length is 0.07 and the Prandtl number is 23.1. It can be seen that the shape of the dendrite is significantly influenced by the flow. The growth velocities of the upstream tips are much higher than of the downstream tips and the tips normal to the flow, because the impinging flow reduces the thermal boundary layer thickness. The evolution of the downstream branch in the wake of the dendrite is retarded relative to the diffusion case, because of advection of heat from the upstream portions of the dendrite. An interesting observation is that the horizontal branches grow slightly upwards. This dendrite "tilting" is due to the asymmetry of the heat fluxes on the sides of the horizontal branches.

The upstream tip eventually reaches a steady state where the tip velocity and curvature do not change with time. Measuring the steady tip velocity, V, and radius, ρ, of the upper tip from the computed phase-field allows for an examination of the dendrite tip operating state in the presence of convection. It is well know from microscopic solvability theory that the product $\rho^2 V$ is a constant that can be nondimensionalized such that it depends only on the anisotropy strength. This dimensionless selection constant is the same for all supercoolings, but it can depend on the flow velocity. Figure 2 shows the ratio of $\rho^2 V$ with flow to the corresponding value without flow as a function of a dimensionless parameter χ that contains the flow Reynolds number among other parameters[3]. A total of 17 computational runs, where the flow velocity, anisotropy strength and supercooling were varied, were performed to obtain this figure. It can be seen that the ratio of selection constants increases with increasing flow strength. All results collapse along a single line. This line is obtained from the microscopic solvability theory with flow of Bouissou and Pelce[3].

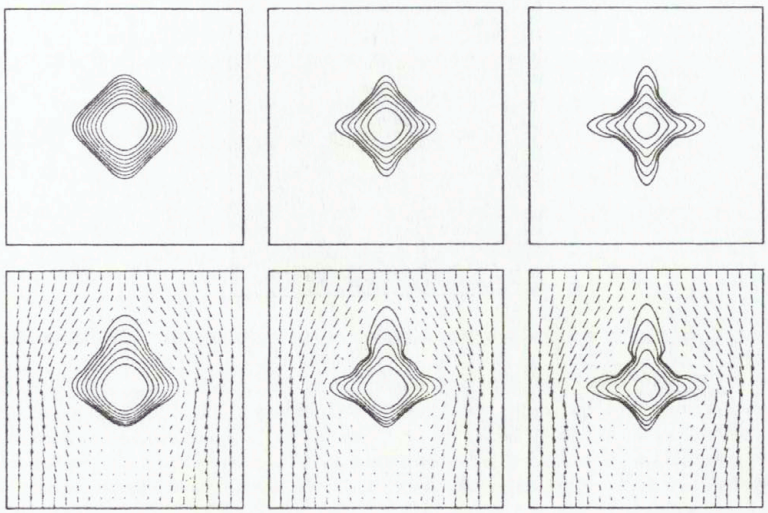

Figure 1. Evolution of phase-filed contours for dendrites growing at a supercooling of 0.55 and three anisotropy strengths (0.01, 0.03, and 0.05 from left to right) without convection (top panels) and with convection (bottom panels)

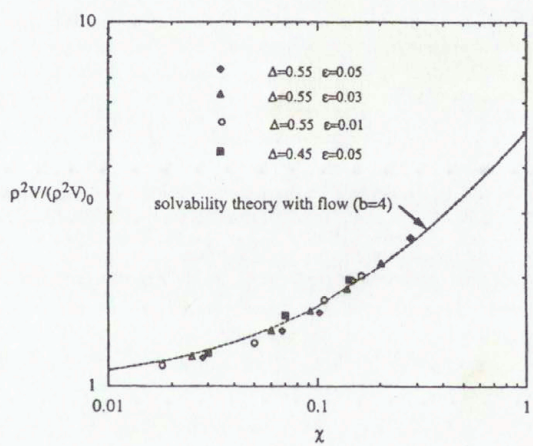

Figure 2. Predicted ratio of the selection constant ρ^2V with flow to without flow as a function of the dimensionless flow parameter χ and comparison with microscopic solvability theory[3]

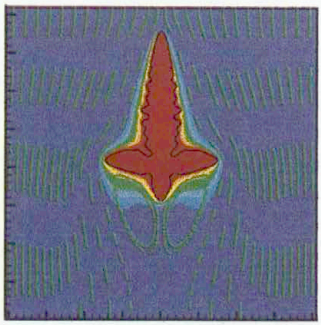

Figure 3. Example of simulated dendritic growth with convection in the presence of thermal noise

Finally, Figure 3 shows the results of a computational run where we introduced stochastic noise into the energy equation according to a method developed by one of the co-authors (AK). The supercooling is 0.55, the anisotropy strength is 3%, the flow Peclet number is 0.135, and the dimensionless noise strength is 0.001. The colours indicate temperature. The upstream tip has grown to a length sufficient for dendrite sidearms to develop. We are presently studying the dependence of the sidearm frequency and amplitude on the flow velocity.

CONCLUSIONS

A phase-field method is presented that allows for the numerical simulation of solidification microstructure development in the presence of flow. Results are presented for two-dimensional equiaxed dendritic growth of a pure substance into a uniformly supercooled melt with and without flow past the crystal. It is found that the growth shape of the dendrite is significantly influenced by the flow. The operating state of the upper (upstream) dendrite tip is investigated in detail and the predictions for the tip velocity and curvature are found to be in good agreement with the microscopic solvability theory with flow of Bouissou and Pelce. Results are also presented for the effect of flow on dendrite sidebranching.

REFERENCES

1. Diepers, H.-J., Beckermann, C., and Steinbach, I.: A Phase-Field Method for Alloy Solidification with Convection. *Solidification Processing 1997*, edited by J. Beech and H. Jones (University of Sheffield, UK, 1997), p. 426.
2. Beckermann, C., Diepers, H.-J., Steinbach, I., Karma, A., and Tong, X.: Modeling Melt Convection in Phase-Field Simulations of Solidification. *J. Computational Physics* (submitted) 1998.
3. Bouissou, P., and Pelcé, P.: Effect of Forced Flow on Dendritic Growth. *Phys. Rev. A* **40**, 6673, 1989.

MELTING IN ENCLOSURES : COUPLED HEAT TRANSFER AND NATURAL CONVECTION

A synthesis of a numerical comparison exercise.

D. GOBIN[1] and P. Le QUÉRÉ[2]

[1] *FAST - UMR 7608. Université Paris-Sud. Bât. 502. 91405 - Orsay (France)*

[2] *LIMSI - UPR 3251. Université Paris-Sud. Bât. 508. 91403 - Orsay (France)*

1. INTRODUCTION

The interest for the numerical simulation of the interaction between phase change and fluid flow is motivated by the wide range of industrial or natural processes where the understanding and modelling of such coupling are of importance. Our interest is to propose a numerical exercise to compare different physical models and numerical procedures on a relatively simple problem, where melting is driven by laminar thermal convection in the melt.

This project takes place after several attempts to compare different numerical procedures (Lacroix and Voller, 1990 ; Viswanath and Jaluria, 1993). Existing experimental results are either too limited in the range of parameters (Bénard *et al.*, 1986) or show significant differences between independent studies (Gau and Viskanta, 1986 ; Campbell & Koster,1994). As a consequence, a purely numerical comparison exercise is proposed, which is intended to provide a set of results in a common framework in order to analyse in detail the characteristics of the numerical solutions in 2D natural convection dominated melting processes, over a wide range of governing parameters. This presentation is a second synthesis based on various contributions from different countries.

2. DESCRIPTION

2.1. Problem Definition

The problem under consideration deals with melting of a pure substance controlled by natural convection in the melt. One considers a 2D square cavity (height H = width L) initially filled with a solid material at a uniform temperature ($T_0 = T_F$). At t* = 0, the temperature of one of the vertical walls (the left wall in *figure 1*) is raised at a value $T_1 > T_F$, while the other vertical wall is maintained at the initial temperature. The horizontal walls are assumed to be adiabatic and no-slip. The fluid flow is supposed to be in the laminar regime, and the thermophysical properties of the material to be constant.

After a pure conduction stage, thermal convection develops in the liquid phase, causing a non-uniform distribution of the heat flux at the interface and a non-uniform displacement of the melting front.

The problem is characterized a set of four main dimensionless parameters. The fluid phase is defined by its Prandtl number : $Pr = \nu/\alpha$ and the intensity of natural convection is given by the thermal Rayleigh number : $Ra = \dfrac{g\beta(T_1 - T_F)H^3}{\alpha\nu}$. Given the temperature conditions, the Stefan number defines the relative importance of the latent heat in the overall energy balance : $Ste = \dfrac{C_{PL}(T_1 - T_F)}{L_F}$. Finally the global aspect ratio of the enclosure has to be specified : $A = H/L$.

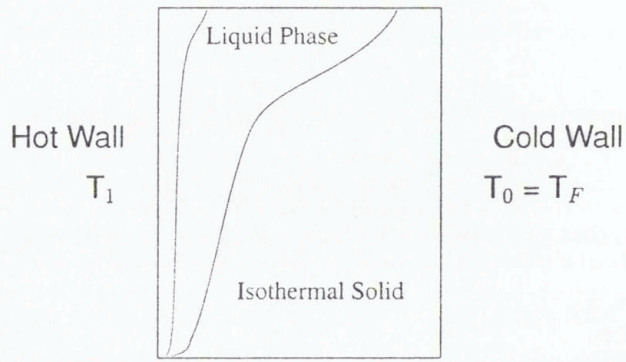

Figure 1. Schematic diagram of the problem.

2.2. Proposed test cases

Two groups of numerical tests heve been proposed, corresponding to distinct ranges of the liquid phase Prandtl number : the *low* Prandtl number range (Pr $\sim 10^{-2}$, melting of metals) and the *high* Prandtl number range (Pr $\sim 10^{2}$, melting of paraffin waxes).

The governing parameters have been estimated using approximate values of the thermophysical properties of tin and octadecane. For a given geometry (A = 1), the values of the Rayleigh and Stefan numbers correspond to a dimensional height of the enclosure H = 0.10 m and a reference temperature difference T_1 - T_F = 3 °C for tin (Case 2) and 10 °C for octadecane (Case 4), leading to the values displayed in Table 1. In each Pr range a 10 times smaller Rayleigh number (Cases 1 and 3) is also considered.

Pr = 0.02 Ste = 0.01	1. Ra = 2.5 10^4 Case 1	2. Ra = 2.5 10^5 Case 2
Pr = 50 Ste = 0.1	3. Ra = 10^7 Case 3	4. Ra = 10^8 Case 4

Table 1. Parameters of the test cases.

In order to limit the outputs, the following results are requested :

1. the time evolution of the melted volume and of the average Nusselt number at the hot wall,
2. the position of the melting front and the local Nusselt number distribution at four different times (expressed in the dimensionless form $\tau = Fo \times Ste = \alpha t^* \times Ste/H^2$:

- at Pr = 0.02 : $t_1 = 4 \times 10^{-3}$, $t_2 = 10^{-2}$, $t_3 = 4 \times 10^{-2}$ and $t_4 = 10^{-1}$
- at Pr = 50 : $t_1 = 5 \times 10^{-4}$, $t_2 = 2 \times 10^{-3}$, $t_3 = 6 \times 10^{-3}$ and $t_4 = 10^{-2}$.

3. HEAT TRANSFER CORRELATIONS

Early studies concerning the characteristic scales of the problem have been performed by Webb & Viskanta (1985) and Beckermann & Viskanta (1989). A more complete description of the problem and an analysis of the relevant parameters and of the scaling laws may be found in the paper by Jany and Bejan (1988). The main features are described in this section.

In the first stage of the melting process, pure conduction is the dominating heat transfer mechanism. The interface moves parallel to the hot wall, and the time evolution of the front position is given by the classical solution of the Stefan problem ($s(t) \sim \sqrt{t}$). Accordingly the Nusselt number decreases like $1/\sqrt{t}$. Then, as the thickness of the liquid layer grows with time, the influence of convection on heat transfer is felt in the top part of the enclosure and progressively along the whole interface. In this transition regime, the competition between pure conduction and natural convection limits the Nusselt number decrease, which goes through a minimum, and then increases when the heat transfer regime is dominated by convection. Finally the boundary layers in the liquid separate and the average heat transfer reaches a constant value.

This analysis was carried out in the high Pr number range, and Jany & Bejan (1989) show that the different time scales and heat transfer rates are readily expressed in terms of power laws of the Rayleigh number. The same approach may be extended to the range of low Pr numbers, where the relevant governing parameter is shown to be the dimensionless group Ra × Pr.

The scaling laws lead to correlations for the evolution of the average Nusselt number as a function of time (τ = Fo Ste), the value of the coefficients are identified from the results of numerical simulations.

1. In the range Pr $\geq$ 1 :

$$Nu(\tau) = \frac{1}{\sqrt{2\tau}} + \frac{Nu_\infty - 1/\sqrt{2\tau}}{\sqrt{1 + \dfrac{1}{(0.0175\, Ra^{3/4}\, \tau^{3/2})^2}}} \,. \tag{1}$$

2. In the range Pr << 1 :

$$Nu(\tau) = Nu_\infty + \frac{1}{\sqrt{2\tau}} \left[1 - \frac{1}{\sqrt{1 + \dfrac{1}{((Ra.Pr)^{0.36}\, \tau^{0.75})^2}}} \right] . \tag{2}$$

Where Nu_∞ is given by the expressions $Nu_\infty = 0.33\, Ra^{0.25}$ in the Pr >> 1 range according to Bénard *et al.* (1985) and $Nu_\infty = 0.29\, Ra^{0.27}\, Pr^{0.18}$ in the Pr << 1 range (Gobin and Bénard, 1992), or by the more general correlation proposed by Lim and Bejan (1992) for any value of Pr :

$$Nu_\infty = \frac{0.35\, Ra^{1/4}}{\left[1 + (0.143/Pr)^{9/16}\right]^{4/9}} \,. \tag{3}$$

4. PRESENTATION OF THE RESULTS

Contributions to the benchmark have been initially requested in the frame of a network of french research laboratories concerned with the simulation of heat and mass transfer processes (AMETH). The call for contribution to the comparison exercise has then been announced in different international journals concerned with heat and mass transfer (*International Journal of Heat and Mass Transfer, Numerical Heat Transfer, International Journal of Thermal Sciences*). The present edition of the exercise has concerned the contributions listed in Table 2.

Author	Laboratory	Cas2
B. BASU A.K. SINGH	TRDDC-Pune (India)	2-3
O. BERTRAND E. ARQUIS	MASTER-Bordeaux (France)	2
B. BINET	THERMAUS-Sherbrooke (Quebec)	1-2-3-4
H. COMBEAU	LSGMM-Nancy (France)	1-2
S.COUTURIER H. SADAT	LET-Poitiers (France)	1-2-3
Y. DELANNOY	EPM/MADYLAM-Grenoble (France)	3-4
D. GOBIN G. VIEIRA	FAST-Orsay (France)	2-3-4
J. GOSCIK	Bialystok University (Poland)	2-3
M. LACROIX	THERMAUS-Sherbrooke (Quebec)	1-2-3-4
P. Le QUÉRÉ	LIMSI-Orsay (France)	1-2-3-4
M. MÉDALE	IUSTI-Marseille (France)	1-2-3
J. MENCINGER B. ŠARLER	LFDT-Ljubljana (Slovenia)	1-2
I. WINTRUFF	IKE-Leopoldshafen (Germany)	1-2-3-4

Table 2. Contributions to the present benchmark.

In the final synthesis, the results will be in terms of three main outputs :
1. the time evolution of the average Nusselt number at the hot wall obtained by the contributors, compared to the Neumann solution and to the existing correlation recalled in section 3,
2. the time evolution of the liquid fraction (the dimensionless melted volume),
3. the position of the melting front at four different times of the process.

To allow for the reception of last minute results, the contributions will be compiled at the last moment, so no results are presented in this text.

Among the 13 sets of results received, most contributions have used fixed grid or "enthalpy" methods (FG) and two have used a front-tracking of transformed grid procedure (TG). Contributions have been requested from groups using commercial softwares, and only one participation has been recorded (FLUENT™ : Delannoy). Twelve contributions have presented results for Case #2, ten for Case #3 and six for Case #4. Only four contributors have solved the four problems.

It will be seen in the presentation that the simulations at high Prandtl numbers globally indicate the same trends, although they may significantly differ due to grid refinement or solution procedure. In the low Prandtl number range however, it will be seen that this exercise has been an opportunity to analyze in more details the melting process for metals and that possible instabilities may take place during the process. This will be presented in a separate paper.[1]

NOMENCLATURE

A	:	aspect ratio of the enclosure, H/L
g	:	acceleration of gravity
Gr	:	Grashof number, $g\,\beta_T\,\Delta T\,H^3/\nu^2$
H	:	height of the enclosure
$\vec{k}$	:	unit vector in the vertical direction
k	:	thermal conductivity of the liquid
L	:	width of the enclosure
Nu	:	average Nusselt number
P	:	dimensionless pressure
Pr	:	Prandtl number, ν/α
Ra	:	Rayleigh number, Pr Gr
Ste	:	Stefan number,
T	:	dimensional temperature
$\vec{V}$	:	dimensionless fluid velocity ($\vec{v^*}\,H/\nu$)
$w\,(u)$	:	vertical (horizontal) component of $\vec{V}$
$x\,(z)$	:	dimensionless coordinates, x^*/H (z^*/H)

Greek symbols

α	:	thermal diffusivity
β_T	:	coefficient of volumetric thermal expansion
ΔT	:	temperature difference between walls
ν	:	kinematic viscosity
ρ	:	fluid density
θ	:	dimensionless temperature, $\theta = (T - T_0)/\Delta T$

REFERENCES

• BECKERMANN C., VISKANTA R. (1989) : Effect of solid subcooling on natural convection melting of a pure metal. *J. Heat Transfer*, **111**, 416–424.

• BÉNARD C., GOBIN D. & MARTINEZ F. (1985) : Melting in rectangular enclosures : experiments and numerical simulations. *J. Heat Transfer*, **107**, 794–803.

• CAMPBELL T.A. & KOSTER J.N. (1994) : Visualization of solid-liquid interface morphologies in gallium subject to natural convection. *J. Crystal Growth*, **140**, 414–425.

• GAU C. & VISKANTA R. (1986) : Melting and solidification of a pure metal from a vertical wall. *J. Heat Transfer*, **108**, 174–181.

• GOBIN D. & BÉNARD C. (1992) : Melting of metals driven by natural convection in the melt : influence of the Prandtl and Rayleigh numbers. *J. Heat Transfer*, **114**, 521–524.

• JANY P. & BEJAN A. (1988) : Scaling theory of melting with natural convection in an enclosure.

[1] A note on possible flow instabilities in melting from the side (Session #8).

Int. J. Heat Mass Transfer, **31**, 1221–1235.

• LACROIX M. & VOLLER V.R. (1990) : Finite difference solutions of solidification phase change problems : transformed vs. fixed grids. *Num. Heat Transfer*, B-**17**, 25–41.

• LIM J.S. & BEJAN A. (1992) : The Prandtl number effect on melting dominated by natural convection. *J. Heat Transfer*, **114**, 784–787.

• VISWANATH R. & JALURIA Y. (1993) : A comparison of different solution methodologies for melting and solidification problems in enclosures. *Num. Heat Transfer*, B-**24**, 77–105.

• WEBB B.W. & VISKANTA R. (1985) : On the characteristic length scale for correlating melting heat transfer data. *Int. Comm. Heat Mass Transfer*, **12**, 637–646.

SOLIDIFICATION AND MELTING IN MICROGRAVITY

E. Leonardi

School of Mechanical and Manufacturing Engineering
The University of New South Wales
Sydney, Australia 2052

Summary Recent modelling work of the solidification and melting of a weak binary alloy in a horizontal Bridgman furnace is presented. The work has been undertaken in connection with the MEPHISTO-4 program, which is a study of the solidification and melting of an alloy of bismuth with 1 at% tin in a microgravity environment. The effects of coupling with the phase diagram (a concentration-dependent melting temperature) and of thermal and solutal convection on segregation of solute, shape and position of the solid/liquid interface are investigated. The results presented include calculations at 1 and 10 μg, both neglecting and including the dependence of melting temperature on concentration.

INTRODUCTION

The investigation of solidification processes has great practical importance for crystal growth techniques. The quality of single crystals grown from the melt depends strongly on growth morphology and macro-segregation caused by convection effects in solidified ingots. A low gravity environment is often used for fundamental studies of crystal growth because it produces conditions in which convection is eliminated or at least decreased to a level at which crystal growth is largely controlled by diffusion. Residual accelerations in orbiting space vehicles are of the order of one to several hundred μg (where 1 μg $=9.81\times10^{-6}$ ms^{-2}). For this reason, much effort has been expended in recent years in performing crystal growth experiments in the microgravity environment of a spacecraft in earth orbit. Such effects as compositional and kinetic supercooling, and the influence of convection on compositional distribution in the melt, have been investigated under microgravity.

The MEPHISTO-4 Program is a joint US-French-Australian research effort directed towards gaining a detailed understanding of the role of buoyancy-driven convection during the directional solidification of faceted materials in a Bridgman apparatus, specifically an alloy of bismuth with 1 at% tin. It combines ground-based experiments and a series of experiments conducted in a microgravity environment. Part of this program is the numerical modelling of the solidification and melting processes.

The MEPHISTO apparatus, shown schematically in Figure 1, consists of three parallel tubes or ampoules (only one is shown in the figure), each containing the Bi-Sn alloy, around which are placed two "furnaces", each comprising a pair of heating and cooling jackets. Between each heating and cooling jacket is a nominally adiabatic or insulated zone. One furnace is fixed, and acts to generate a reference state; the other can be moved over the tubes. If it moves in the direction from the cooling to the heating jacket (*i.e.*, to the right in Figure 1), and if the heating and cooling rates are chosen appropriately, the material will be progressively solidified from left to right.

In the Bridgman configuration with low growth speeds and high thermal gradients in the adiabatic zone, the interface stays sharp and phase change is isothermal; *i.e.*, there is no mushy zone or

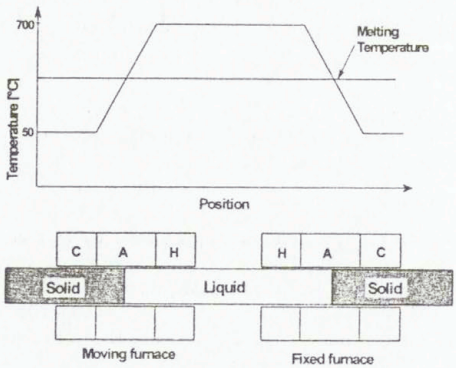

Figure 1. Schematic diagram of the MEPHISTO apparatus. H and C denote the hot and cold sections of the furnaces; A denotes the adiabatic zone.

transition region between the solid and the liquid. Implementation of a fixed grid single domain approach (commonly called the enthalpy method) for modelling the isothermal phase change of alloys becomes quite a challenging problem because of the additional difficulties associated with the discontinuity of solute concentration at the interface and the sharp gradients of concentration at the interface, induced by the low value of partition coefficient. These are the conditions, which apply in MEPHISTO.

MATHEMATICAL MODEL

We consider a Bridgman furnace in which a moving temperature profile consisting of a cold zone (T_c), a nominally adiabatic zone and a hot zone (T_h) is imposed on the boundary of the ampoule. This boundary temperature profile is translated with a constant pulling velocity, as a result of the furnace movement, causing the solid/liquid interface to move along the ampoule. The material in the ampoule is thus divided into two sub-regions: solid and liquid.

The velocity, temperature and solute distributions in the solid and liquid regions are obtained by solving the equations of motion, energy and concentration.

A vorticity/stream function formulation is used, in which the continuity equation is automatically satisfied and the pressure is omitted as a solution variable. Applying a modified Boussinesq approximation, the governing equations of motion become,

$$\rho\left(\frac{\partial \zeta}{\partial t} + \nabla.\left(\vec{V}\,\zeta\right)\right) = \nabla\rho \times \hat{g}|g| + \mu\nabla^2\zeta \qquad (1)$$

$$\nabla \times \psi = -\zeta \qquad (2)$$

where ρ, μ, ζ, ψ and $\vec{V}$ are respectively the density, viscosity, vorticity, stream function and velocity vector; g is the magnitude of the gravitational acceleration, and $\hat{g}$ is the unit vector in the direction of gravity. The density in the buoyancy term of equation (1) is assumed to be a linear

function of temperature and solute concentration:

$$\rho = \rho_r \left[1 - \beta_T \left(T - T_r\right) + \beta_C \left(C - C_r\right)\right] \tag{3}$$

where β_T and β_C are the (assumed constant) thermal and solutal expansion coefficients, defined by

$$\beta_T = -\frac{1}{\rho_r}\frac{\partial \rho}{\partial T} \quad \text{and} \quad \beta_C = \frac{1}{\rho_r}\frac{\partial \rho}{\partial C} \tag{4), (5}$$

ρ_r, T_r and C_r are reference values of density, temperature and concentration.

The energy equation can be written as[1]:

$$\rho\left[C^*(T)\frac{\partial T}{\partial t} + c_p \nabla\left(\tilde{V}T\right)\right] = \lambda \nabla^2 T\,, \tag{6}$$

in which c_p, λ and T are respectively the specific heat, thermal conductivity and temperature. To account for the latent heat evolution during phase change we introduce an effective specific heat[2], $C^*(T)$, given by:

$$C^*(T) \equiv \frac{\partial h}{\partial T} = c_p + L\frac{\partial f_\ell}{\partial T} \tag{7}$$

where L is the latent heat and f_ℓ is a local liquid volume fraction.

As the temperature distribution on the boundary and hence the solid/liquid interface moves, the solid sub-region of the computational domain increases in length. In the solid, the vorticity, stream function and velocities are set to zero. In the liquid, they are calculated from the stream function defined as:

$$\tilde{V} = \nabla \times \tilde{\psi}\,. \tag{8}$$

The most difficult problem in modelling solute transport during solidification is associated with the discontinuity of solute concentration at the interface. Additional difficulties occur due to the presence of a thin solute boundary layer in the liquid in which large solute gradients develop, induced by the low partition coefficient.

The basic assumptions in the analysis are:

- Thermodynamic equilibrium exists at the solid-liquid interface: $T_m = T_s = T_\ell$ and $C_s = k_p C_\ell$, where T_m is the melting temperature, the subscripts s and ℓ denote solid and liquid, and k_p is the partition coefficient;
- Solute diffusion in the solid phase is negligible;
- The solid phase is stationary and a distinct separation of the phases exists at the interface;
- The densities and thermal conductivities[†] of the liquid and solid phases are constant and equal.

The solute transport equation can be written as[1]:

$$\frac{\partial C_\ell}{\partial t} + \nabla\left(\tilde{V}C_\ell\right) = D\,\nabla^2 C_\ell + \left[\frac{\partial f_s}{\partial t}(1 - k_p)C_\ell + f_s\frac{\partial C_\ell}{\partial t}\right] \tag{9}$$

[†] In more recent work we have included unequal thermal conductivities.

where C_ℓ and D are respectively the liquid concentration and diffusivity of the solute. The term in the square brackets is a source term introduced to account for the release of solute into the liquid during solidification[1]; $f_s = 1 - f_\ell$ is the local solid volume fraction. Equation (9) applies to the liquid concentration only and hence bypass the concentration discontinuity at the interface.

During the initial transients of solidification, the melting temperature varies with time due to changes in the concentration of the solute. With the assumption that phase change takes place under local thermodynamic equilibrium, the temperature at the interface – the melting temperature $T_m(C)$ – can be expressed as:

$$T_m(C) = T_{m0} + mC_I \tag{10}$$

where T_{m0} is the melting temperature of pure solvent, C_I is the interface solute concentration and m is slope of the liquidus, assumed to be constant and obtained from the phase diagram.

During melting, it is assumed that the interface solute concentration on the liquid side is equal to that on the solid side[3]. The equilibrium condition $C_s = k_p C_\ell$ is supposed to be satisfied by the creation of a thin layer of molecular scale in the solid which we have not attempted to model.

SOLUTION METHOD

An algorithm entitled SOLCON[‡], which incorporates the closely coupled solution of the transport equations in a vorticity-stream function formulation, was developed. In this algorithm, a modified alternating direction implicit (ADI) Samarskii-Andreyev scheme[4] is used to solve iteratively the vorticity, stream function, energy and solutal equations at each time step. The modification achieves accurate coupling between the transient equations and the boundary conditions and hence a true transient "simultaneous" solution of the equations. Since the temperature boundary profile is moving in discrete time steps, obtaining an accurate true transient solution is impossible without having all equations converged at each time step. Apart from that, the use of iterations becomes necessary because of the strong non-linearity of all governing equations. To ensure stability of the computational process, all source terms and non-linear coefficients depending on liquid fraction are linearised based on the value of liquid fraction obtained from the previous iteration.

The vorticity, stream function and energy equations were discretised using central differences and solved by the modified ADI scheme with internal iterations. Interface boundary conditions for vorticity and stream function were applied at those mesh points in the solid sub-region which are adjacent to the liquid. For the calculation of vorticity boundary conditions, the definition of vorticity was used: $\tilde{\zeta} = \nabla \times \tilde{V}$. The boundary condition $\psi = 0$ was used for the stream function.

The concentration equation (9) required special treatment. It was discretised and solved using a control volume approach. This ensures mass balance during phase change in the partially solidified control volume.

To resolve the sharp gradients of concentration in the vicinity of interface, a second order upwind scheme[5] was used to discretise the convection fluxes. This was chosen because it is more stable than central differences, particularly for problems with low diffusion coefficients. Central differences were used for the diffusion terms.

---

‡ SOLidification and CONvection

To account for the interface movement through the partially solidified control volume, the diffusion flux in the direction of solidification, $q'_{i+1/2,j}$, integrated over the control volume face Δy, was written as

$$q'_{i+1/2,j} = D'_{i+1/2,j} \frac{C'_{i+1,j} - C'_{i,j}}{\Delta x^*} \Delta y \qquad (11)$$

where $\Delta x^* = 0.5\ (f_r + 1)\ \Delta x$ is the distance between the centre of the liquid portion of a partially solidified control volume and the centre of the next control volume. Convection and diffusion fluxes in the direction normal to solidification have been integrated over liquid fractions of the control volume faces $f_r \Delta x$.

The computed solute concentration can oscillate when the phase change front moves from one cell into the next. The reason is that in a fixed grid finite volume formulation, the computed values of C are cell averaged values. As the interface moves from one cell to the next, C suddenly drops from one value to a lower value. The concentration in the new cell then increases due to progressive solute rejection at the interface, which occurs at a rate faster than diffusion out of the control volume. The problem becomes even more difficult when variations of melting temperature with solute concentration are taken into account. The concentration-dependent melting temperature obtained from equation (10) will have an unrealistic zigzag shape and hence will not be suitable for the calculation of the liquid fraction and the estimation of interface position. To overcome this problem and to account for the fact that the computed concentration is a cell average value, an exponential extrapolation procedure based on the liquid fraction has been introduced to determine the value of the concentration at the solid/liquid interface[6].

RESULTS AND DISCUSSION

Calculations were made for an ampoule 42 mm long and 6 mm across. The gravity vector was taken to be acting in a direction normal to the x-axis of the ampoule. Solutions have been obtained for both 1 μg and 10 μg. The property values of pure liquid bismuth at a reference temperature of 271.3 °C (the equilibrium melting temperature) were used[1].

The computational domain initially contained only liquid Bi with a uniform solute concentration C_0 of 1 at% Sn and a uniform temperature of 700 °C. The cold end of the ampoule (the left end) had an initial temperature of 272 °C. Along the top and bottom boundaries, the temperature increased from the left at 20 K/mm and continued over a length of 21.4 mm until 700 °C was reached. From that position onward, the temperature remained constant. The right end of the computational domain had a constant temperature of 700 °C. Numerical experimentation showed that the presence of a wall at 42 mm had no effect on the solidification or the flow near the interface for the few mm of solid that were formed.

The pulling velocity – the rate of translation of the boundary temperature distribution – was 3.34 μm/s (one of the values used in the MEPHISTO experiment), and was also imposed from $t > 0$. Solidification occurred from left to right as time progressed. The cold end temperature decreased with time in accordance with the imposed temperature gradient until a minimum value of 50 °C was reached; thereafter it was kept at 50 °C. This temperature distribution was imposed at the liquid

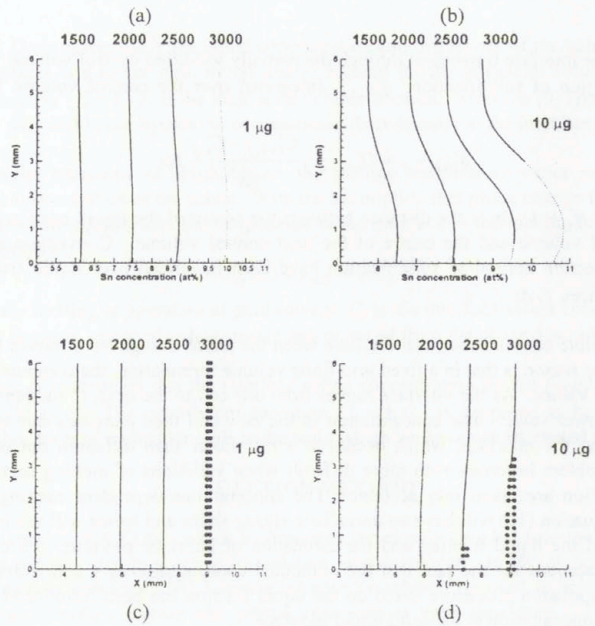

Figure 2. Distribution of solute concentration across the interface (a and b), and position of the interface (c and d) at 1500, 2000, 2500 and 3000 sec for 1 μg and 10 μg. Dotted lines indicate instability of the plane front.

boundary, *i.e.*, conduction in the ampoule was not considered[§]. A uniform square mesh of 210×30 cells (0.2×0.2 mm) was used. The computations were performed for 3000 seconds of solidification.

Figure 2 shows the effect of the magnitude of g on the distribution of solute concentration along the interface (a and b) and position of the interface (c and d) at 1500, 2000, 2500 and 3000 sec.

After about 2800 seconds of solidification, the results showed oscillations in the interface solute concentration, C_i, which can be explained by considering the condition necessary for stable plane front solidification. According to the theory of constitutional supercooling (*e.g.*, Flemings[7]), instability of the plane front (leading to a cellular interface) can occur when the liquid immediately in front of the interface has a temperature which is below its equilibrium liquidus temperature (*i.e.*, below its melting temperature). In this condition, the liquid is said to be supercooled. Constitutional supercooling will not occur when the actual temperature gradient in the liquid in

[§] In more recent work we have included conduction in the quartz ampoule as part of the calculation procedure, and have imposed a temperature gradient of 27 K/mm on the outside of the ampoule. This leads to an internal gradient of approximately 20 K/mm, as used here. The isotherms in the sample remain virtually orthogonal to the ampoule axis, although not in the ampoule itself, which has a much lower thermal conductivity.

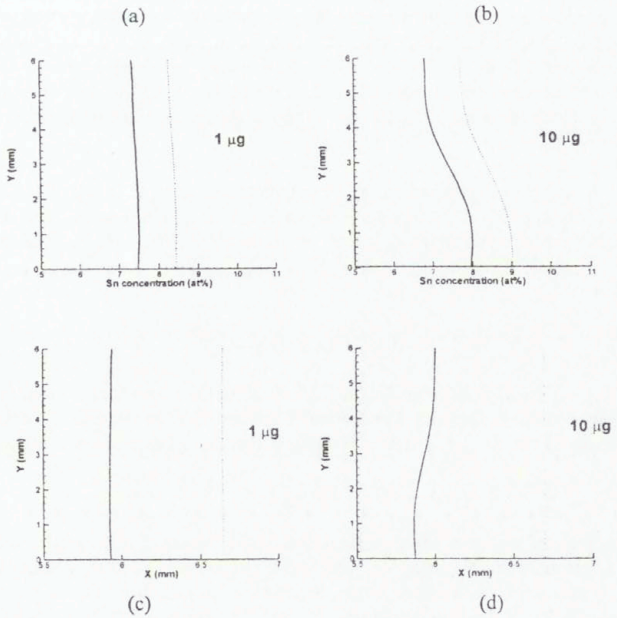

Figure 3. Distribution of solute concentration along the interface (a and b), and position of the interface (c and d) after 2000 sec of solidification for constant (dashed lines) and concentration-dependent (solid lines) melting temperature for 1 μg and 10 μg.

front of the interface is equal to or greater than the melting temperature gradient corresponding to the local solute concentration gradient.

Dashed lines in Figure 2 (a) and (b) correspond to the parts of the interface at which instability of the plane front appeared and in front of which supercooled liquid existed. These regions are shown by dots in Figure 2 (c) and (d), which identify the adjacent control volumes in both of which solidification is occurring. Instability appears earlier at 10 μg due to the higher solute segregation which builds up at the interface. By 2500 seconds, the segregation of solute at the interface at 10 μg was 20.6 % whereas for 1 μg it was 2.65%. The segregation at 10 μg is such that the concentration near the bottom of the cavity exceeds 9.4 at% (Figure 2(b)) while at 1 μg the concentration remains less than 8.7% as shown in Figure 2(a).

The numerical solutions show instability occurring when the solute concentration exceeds 9.4 at%, whilst it can be shown[6] that the estimated critical concentration is $(C_l)_{cr} = 9.2$ at%.

Values of solute concentration at the interface and the position and shape of the interface after 2000 seconds of solidification are shown in Figure 3 for two values of g and for constant (dashed lines) and concentration-dependent (solid lines) melting temperature. Although the inclusion of a

concentration-dependent melting temperature in the computations has a large effect on the shape and position of the interface, it has only a small effect on the segregation at the interface, changing it from 17.05% for constant T_m to 16.05% for variable T_m at 10 μg, and from 1.99% to 1.97% at 1 μg respectively. Segregation is more strongly affected by the gravity level. Values of concentration at the interface are smaller in the case of $T_m(C)$ due to the shorter distance of solidification as indicated in Fig. 3 (c), (d).

If T_m is constant, the interface is represented by an isotherm and remains virtually flat (*i.e.* parallel to the y axis). However, when T_m is concentration-dependent, segregation (especially at 10 μg) causes the interface to be curved, and it is no longer an isotherm. Differences in the shape of the solid/liquid interface determined by differences in the segregation at 1 and 10 μg can be seen in Figure 3 (c) and (d).

CONCLUSION

The results show clearly that it is important to include the effect of solute concentration on the melting temperature in the solidification simulation. The velocity of the interface is determined not just by the pulling speed but also by the rate at which the interface concentration is increasing.

ACKNOWLEDGEMENTS

This research is being undertaken in the Computational Fluid Dynamics Research Laboratory of the School of Mechanical and Manufacturing Engineering of The University of New South Wales. The team members, in addition to the present author, are Professor G. de Vahl Davis, Dr. S.S. Leong, Dr. V. Timchenko, Dr. P.Y.P Chen, and graduate students J. Kaenton and C. Benjapiyaporn.

We acknowledge with thanks the support of the Australian Research Council. We also express our gratitude to Professor Reza Abbaschian, University of Florida (Principal Investigator) for the opportunity to participate in MEPHISTO-4, and for his continual guidance during this research, and to Mr Henry de Groh III, NASA Lewis Research Center (NASA Project Scientist for MEPHISTO-4), for his close co-operation.

REFERENCES

1. Timchenko, V., Chen, P.Y.P., de Vahl Davis, G., Leonardi, E. and de Groh III, H.C.: Directional Solidification in Microgravity, *Heat Transfer 98*, J.S. Lee (ed.), Taylor & Francis, pp. 241-246, 1998.
2. Morgan, K., Lewis, R.W. and Zienkiewicz, O.C.: An improved algorithm for heat conduction problems with phase change. *Int. J. Numer. Meth. Eng.*, **12**, pp. 1191-1195, 1978.
3. Abbaschian, R., Private communication, 1997.
4. Samarskii, A.A. and Andreyev, V.B.: On a high-accuracy difference scheme for an elliptic equation with several space variables. *USSR Comput. Math. and Math. Phys*, **3**, pp. 1373-1382, 1963.
5. Tamamidis, P. and Assanis, D.N.: Evaluation of various high-order-accuracy schemes with and without flux limiters. *Int J. Num. Methods in Fluids*, **16**, pp. 931-948, 1993.
6. Timchenko, V., Chen, P.Y.P., Leonardi, E., de Vahl Davis, G. and Abbaschian, R.: A Computational Study of Transient Plane Front Solidification of Alloys in a Bridgman Apparatus under Microgravity Conditions, Accepted for publication in *Int. J. Heat and Mass Transfer*, 1999.
7. Flemings, M.C., *Solidification processing*, McGraw-Hill Inc., pp. 58-61, 1974.

EXISTENCE OF SOLUTIONS TO A PHASE-FIELD MODEL FOR THE ISOTHERMAL SOLIDIFICATION PROCESS OF A BINARY ALLOY *

J. Rappaz [1], J.F. Scheid [2]

Swiss Federal Institute of Technology, EPFL
Department of Mathematics
CH-1015 Lausanne, Switzerland

In this note, we investigate the well-posedness of a solutal phase-field model for the isothermal solidification of a binary alloy [4]. This model due to Warren-Boettinger [5], involves the relative concentration c and an order parameter ϕ which accounts for the solidification state of the alloy by being equal to 0 if the system is in a solid phase and equal to 1 if it is in a liquid phase. The time evolution of c and ϕ is governed by the following equations :

$$(P)\begin{cases} \dfrac{\partial \phi}{\partial t} = \varepsilon^2 \Delta \phi + F_1(\phi) + cF_2(\phi) & \text{in } \Omega \times (0, +\infty), \\ \dfrac{\partial c}{\partial t} = \operatorname{div}\left(D_1(\phi)\nabla c + D_2(c,\phi)\nabla \phi\right) & \text{in } \Omega \times (0, +\infty), \\ \dfrac{\partial \phi}{\partial n} = \dfrac{\partial c}{\partial n} = 0 & \text{on } \partial\Omega \times (0, +\infty), \\ \phi(0) = \phi_0, \quad c(0) = c_0 & \text{in } \Omega, \end{cases}$$

where Ω is an open bounded domain in $\mathbb{R}^d$ with $1 \leq d \leq 3$ and with a smooth boundary $\partial\Omega$, n is the unit normal to $\partial\Omega$ and $\varepsilon > 0$ is a given positive constant.

The functions F_1, F_2 appearing in (P) are given and satisfy $F_i(0) = F_i(1) = 0$ for $i = 1, 2$, function D_1 is bounded from below by a positive constant and function D_2 is such that $D_2(0, \phi) = D_2(1, \phi) = 0$ for $\phi \in [0, 1]$. Moreover, initial physical data c_0 and ϕ_0 are given with values between 0 and 1. The solutions c and ϕ of Problem (P) must be found with the same property.

Phase-field models have been principally used to describe phase transitions of pure materials due to thermal effects and they lead to nonlinear parabolic systems for the phase-field and the temperature (see e.g. [1], [2], [3]). However, the nonlinearities are then different from those of Problem (P).

*supported by the Swiss National Foundation.
[1]email : Jacques.Rappaz@epfl.ch
[2]email : Jean-Francois.Scheid@epfl.ch

WEAK SOLUTIONS

We first prove the existence of weak solutions to Problem (P) under Lipschitz and boundeness assumptions on the nonlinear functions F_i and D_i, $i = 1, 2$. More precisely, we assume that

(H1) · F_1, $F_2 \in C(\mathbb{R})$ are Lipschitz and bounded functions.

(H2) · $D_1 \in C(\mathbb{R})$ is a Lipschitz positive function, bounded above and below by two positive constants.

(H3) · $D_2 \in C(\mathbb{R} \times \mathbb{R})$ is a Lipschitz and bounded function.

We note $V = H^1(\Omega)$ and V' is the dual space $(H^1(\Omega))'$ of $H^1(\Omega)$. We denote by $< . , . >_{V',V}$ the duality product between V' and V. Then the following result holds

Theorem 1 *Let assumptions (H1)-(H3) be fulfilled.*

1) For any $(\phi_0, c_0) \in L^2(\Omega) \times L^2(\Omega)$ and $T > 0$, there exists a couple of functions (ϕ, c) satisfying

$$\phi,\ c \in L^2(0,T;H^1(\Omega)) \cap H^1(0,T;V'),$$

such that $\phi(0) = \phi_0$, $c(0) = c_0$ and

$$\begin{aligned} &< \frac{\partial \phi}{\partial t}, v >_{V',V} + \varepsilon^2 \int_\Omega \nabla \phi \cdot \nabla v \, dx = \int_\Omega (F_1(\phi) + cF_2(\phi))\, v \, dx, \\ &< \frac{\partial c}{\partial t}, w >_{V',V} + \int_\Omega (D_1(\phi)\nabla c + D_2(c,\phi)\nabla \phi) \cdot \nabla w \, dx = 0, \end{aligned} \tag{1}$$

for all $v,\ w \in H^1(\Omega)$ and a.e. in $(0,T)$.

2) For any $(\phi_0, c_0) \in H^1(\Omega) \times L^2(\Omega)$ and $T > 0$, there exists a couple of functions (ϕ, c) satisfying

$$\begin{aligned} &\phi \in L^2(0,T;H^2(\Omega)) \cap H^1(0,T;L^2(\Omega)), \\ &c \in L^2(0,T;H^1(\Omega)) \cap H^1(0,T;V'), \end{aligned}$$

such that $\phi(0) = \phi_0$, $c(0) = c_0$ and

$$\begin{aligned} &\frac{\partial \phi}{\partial t} - \varepsilon^2 \Delta \phi = F_1(\phi) + cF_2(\phi) \qquad \text{a.e. in } \Omega \times (0,T), \\ &\frac{\partial \phi}{\partial n} = 0 \qquad \text{a.e. on } \partial\Omega \times (0,T), \\ &< \frac{\partial c}{\partial t}, v >_{V',V} + \int_\Omega (D_1(\phi)\nabla c + D_2(c,\phi)\nabla \phi) \cdot \nabla v \, dx = 0, \\ &\text{for all } v \in H^1(\Omega) \text{ and a.e. in } (0,T). \end{aligned} \tag{2}$$

REMARK : Since $\phi,\ c \in L^2(0,T;H^1(\Omega)) \cap H^1(0,T;V')$ it follows that $\phi,\ c \in C([0,T];L^2(\Omega))$. Moreover, as soon as $\phi \in L^2(0,T;H^2(\Omega)) \cap H^1(0,T;L^2(\Omega))$, we infer that $\phi \in C([0,T];H^1(\Omega))$.

The proof of Theorem 1 is based on a Faedo-Galerkin method with the use of a finite vector space spanned by the eigenfunctions of the operator $(-\Delta)$ with homogeneous Neumann boundary conditions (see [4]).

REGULARITY AND UNIQUENESS

Under the additional assumption that the initial data are smooth enough, we have the following regularity and uniqueness result

Theorem 2 *Let assumptions (H1)-(H3) be fulfilled.*

Let $\phi_0 \in H^2(\Omega)$ *such that* $\dfrac{\partial \phi_0}{\partial n} = 0$ *on* $\partial\Omega$ *and* $c_0 \in H^1(\Omega)$. *Then for any* $T > 0$, *there exists a unique couple of functions* (ϕ, c) *satisfying*

$$\begin{aligned} &\phi \in L^2(0,T;H^3(\Omega)) \cap H^1(0,T;H^1(\Omega)), \\ &c \in L^2(0,T;H^2(\Omega)) \cap H^1(0,T;L^2(\Omega)), \end{aligned} \tag{3}$$

such that $\phi(0) = \phi_0$, $c(0) = c_0$ *and*

$$\begin{aligned} &\frac{\partial \phi}{\partial t} - \varepsilon^2 \Delta \phi = F_1(\phi) + cF_2(\phi) \qquad \text{a.e. in } \Omega \times (0,T), \\ &\frac{\partial c}{\partial t} = div\,(D_1(\phi)\nabla c + D_2(c,\phi)\nabla \phi) \qquad \text{a.e. in } \Omega \times (0,T), \\ &\frac{\partial \phi}{\partial n} = \frac{\partial c}{\partial n} = 0 \qquad \text{a.e. on } \partial\Omega \times (0,T). \end{aligned} \tag{4}$$

REMARK : We infer from the regularity of the solution that $\phi \in C([0,T];H^2(\Omega))$ and $c \in C([0,T];H^1(\Omega))$.

Theorem 2 is proved by establishing further a priori estimates in the Faedo-Galerkin procedure (see [4]). These estimates are obtained thanks to Gagliardo-Nirenberg inequalities.

A MAXIMUM PRINCIPLE AND CONCLUSION

In order to conclude to the existence of solution to Problem (P) with physical assumptions, we need a maximum principle which is obtained under extra assumptions on the nonlinear terms. More precisely, in addition to (H1) (H2) and (H3), we suppose that the nonlinear terms F_1, F_2, and D_2 satisfy the following extra assumptions :

(H4) · $F_1 \equiv F_2 \equiv 0$ in $]-\infty, 0] \cup [1, +\infty[$.

(H5) · $D_2(\cdot, r_2) \equiv 0$ in $]-\infty, 0] \cup [1, +\infty[$ and for all $r_2 \in \mathbb{R}$.

Then we have the following result

Theorem 3 *Let assumptions (H1)-(H5) be fulfilled.*

Suppose that the initial data $(\phi_0, c_0) \in L^2(\Omega) \times L^2(\Omega)$ *is such that*

$$0 \leq \phi_0(x),\ c_0(x) \leq 1 \text{ for a.e. } x \in \Omega.$$

Then for any $T > 0$, *every weak solution* $(\phi,\ c) \in (L^2(0,T;H^1(\Omega)))^2 \cap (H^1(0,T;V'))^2$ *satisfies for all* $t \in [0,T]$

$$0 \leq \phi(x,t),\ c(x,t) \leq 1 \text{ for a.e. } x \in \Omega.$$

We are now able to conclude to the well-posedness of Problem (P) with physical assumptions for the nonlinear functions F_i, D_i, $i = 1, 2$. In particular, the physical modelling leads to functions F_1 and F_2 depending on ϕ which are polynomial functions of degree 4 with $\phi \in [0, 1]$ and vanishing for $\phi = 0$ and $\phi = 1$. Function D_2 depending on c and ϕ satisfies the relation $D_2(0, \phi) = D_2(1, \phi) = 0$, for all $\phi \in [0, 1]$. When c and ϕ do not belong to interval $[0, 1]$, functions F_1, F_2 and D_2 are not defined. It follows that we consider a vanishing extension of F_1, F_2 beyond the set $\{0 < \phi < 1\}$ and an extension of D_2 to all the values of c and ϕ, satisfying assumption (H3) and vanishing beyond the set $\{0 < c < 1\}$. In that way, we obtain nonlinear functions $\tilde{F}_1$, $\tilde{F}_2$ and $\tilde{D}_2$ satisfying the Lipschitz and boundeness assumptions (H1),(H2),(H3) and then we can apply existence and regularity results of Theorem 1 and Theorem 2. Moreover, since $\tilde{F}_1$, $\tilde{F}_2$ and $\tilde{D}_2$ also satisfy the vanishing assumptions (H4) and (H5), the maximum principle given by Theorem 3 holds and since the initial physical data c_0 and ϕ_0 are values belonging to the interval $[0, 1]$, we are sure that the solution (c, ϕ) remains included between 0 and 1 when the time t goes up. It follows that c and ϕ don't depend on the choice of the extension of functions F_1, F_2, D_2 outside the interval $[0, 1]$ and consequently the physical problem (P) is well-posed.

References

[1] Caginalp G., 'An analysis of a phase-field model for free boundary', *Arch. Rational Mech. Anal.*, **92**, 205-245 (1986).

[2] Elliott C.M., Zheng S., 'Global existence and stability of solutions to the phase-field equations', in *Free Boundary Value Problems*, K. H. Hoffmann, J. Sprekels, eds., Internat. Ser. Num. Math., vol. 95, Birkhäuser, Basel, 1990, pp. 46-58.

[3] Laurençot Ph., 'Weak solutions to a phase-field model with non-constant thermal conductivity', *Quart. Appl. Math.*, **4**, 739-760 (1997).

[4] Rappaz J., Scheid J.F., 'Existence of solutions to a phase-field model for the isothermal solidification process of a binary alloy', submitted to *Math. Methods Appl. Sci.*

[5] Warren J.A., Boettinger W.J., 'Prediction of dendritic growth and microsegregation patterns in a binary alloy using the phase-field model', *Acta metall. mater.*, **43** (2), 689-703 (1995).

SOME INTERFACES BETWEEN THEORY AND EXPERIMENT

David S. Riley

Division of Theoretical Mechanics, School of Mathematical Sciences

University of Nottingham, University Park

Nottingham NG7 2RD, UK

E-mail: david.riley@nottingham.ac.uk

Heat transfer between two media involving liquid-solid phase transitions is important in both nature and industry. Natural situations include ice formation in rivers, melting of icebergs and lava flows from volcanoes. Industrial areas of interest include casting, welding, hot liquid jets for drilling and the design of heat sinks in power generating systems and in the nuclear power industry. In this last example, the operators are required to demonstrate that adequate safety margins exist even under severe accident conditions. This means that the physical processes involved in extreme conditions are sufficiently understood that corrective actions can be implemented effectively.

The problem motivating the current work is an extreme hypothetical situation in a gas-cooled reactor, where it is supposed that the shutdown systems have failed to arrest some event that has led to the fuel in a particular channel to overheat, causing the entire fuel inventory of that channel to melt and pour onto the steel floor below. In a matter of seconds this molten fuel material would spread over the floor and freeze into a solidified mass. On a much longer time-scale, the solidified fuel would release its nuclear decay heat, partly to the gaseous environment (by radiative heat transfer) and partly to the steel floor (by conduction). In considering the possibility of melting of the floor due to the release of this decay heat, the extent of spreading of the molten material is a key factor since this determines the effective strength of the source of heat to the base. In practice the strongest inhibitor to spreading is crust formation on the top of the melt. In this talk, results from two sets of simulant experiments will be presented, distinct flow regimes will be identified and analysed.

The first set of experiments involves the radial flow of a low-Prandtl number metal (cerrobend) over an aluminium substrate. Here the source of the cerrobend is a jet in free-fall from a heated source above the substrate. Over the parameter regime considered the flow is inertia dominated and always features a hydraulic jump. The solidification in this case is effected mainly by basal conduction and there is a little convective cooling of the top surface.

The second set of experiments involves a low-Prandtl number wax (polyethylene glycol) which is extruded under pressure into a bath of coolant containing ethylene glycol such that the dominant cooling is at the melt/coolant interface rather than between the melt and the substrate. This leads to an extensive crusting of the surface and a consequential reduction in the size of the footprint of the spread. This flow regime is viscous-dominated and the crust has a visco-elastic nature.

Motivated by these experimental studies, simple mathematical models, reflecting some of the features, have been developed and analysed. In the inertia-dominated case, shallow-water equations incorporating surface tension effects have been considered,

$$\frac{\partial u}{\partial t} + u\frac{\partial u}{\partial r} + \frac{1}{\mathrm{Fr}}\frac{\partial h}{\partial r} - \sigma\frac{\partial}{\partial r}\left(\frac{1}{r^n}\frac{\partial}{\partial r}\left(r^n\frac{\partial h}{\partial r}\right)\right) = 0$$

$$\frac{\partial h}{\partial t} + \frac{\partial}{\partial r}(uh) + n\frac{uh}{r} = 0$$

where $n = 0$ and 1 in the plane and axisymmetric cases, respectively, u is the velocity component parallel to the substrate, $z = h(r,t)$ denotes the free surface, Fr is the Froude number and σ is a dimensionless surface tension coefficient. While in the viscous case, a lubrication model for a fluid with temperature-dependent viscosity has been investigated,

$$\frac{\partial h}{\partial t} - \frac{1}{3r^n}\frac{\partial}{\partial r}\left(\frac{h^3 r^n}{\mu(T)}\frac{\partial h}{\partial r}\right) = 0,$$

where the viscosity μ is a given function of the temperature $T(r,t)$ and the rest of the notation is as above. Results will be presented for both of these models.